inorganics

MDPI

Article

Adsorption Studies of Ternary Metal Ions (Cs^+, Sr^{2+}, and Co^{2+}) from Water Using Zeolite@Magnetic Nanoparticles ($Z@Fe_3O_4$ NPs)

Tung Van Nguyen [1], Lien Thi Nguyen [1], Ha Thi Thu Nguyen [1] and Thu-Huong Le [2,*]

[1] Institute for Technology of Radioactive and Rare Elements (ITRRE), Hanoi 1000, Vietnam; tungnv.88@gmail.com (T.V.N.); nguyenlien1507@gmail.com (L.T.N.); ha3007.au@gmail.com (H.T.T.N.)
[2] Faculty of Chemistry and Environment, Thuyloi University, Hanoi 1000, Vietnam
* Correspondence: lethuhuong@tlu.edu.vn

Abstract: The mixture of three metal ions (Cs^+, Sr^{2+}, and Co^{2+}) is commonly found in radioactive waste, which induces several negative health effects. The removal of multiple metal ions is a true challenge for researchers due to the competitive adsorption of ions onto adsorbents. In this study, three metal ions, namely Cs^+, Sr^{2+}, and Co^{2+}, have been successfully removed simultaneously from water using zeolite@magnetic nanoparticles ($Z@Fe_3O_4$ NPs). The optimized condition for the adsorption of ternary metal ions was obtained at an adsorbent weight of 0.2, pH of 6.0~7.0, and contact time of 60 min. The adsorption mechanism of ternary metal ions onto the surface of $Z@Fe_3O_4$ NPs was studied using the Pseudo-first-order, Pseudo-second-order, Elovich, and Intra-particle diffusion models. The Dubinin–Radushkevich Temkin, Freundlich, and Langmuir isotherm models were used to study the isotherm adsorption. The ternary metal ion adsorption (Cs^+, Sr^{2+}, and Co^{2+}) on $Z@Fe_3O_4$ NPs was followed by the Pseudo-second-order model (PSO) with correlation coefficient (R^2) range of 0.9826–0.9997. Meanwhile, the adsorption isotherms of ternary metal ions on $Z@Fe_3O_4$ NPs were in line with the Langmuir model with R^2 values higher than 0.9206, suggesting monolayer chemisorption with maximum adsorption capacities of 48.31, 15.02, and 10.41 mg/g for Cs^+, Sr^{2+}, and Co^{2+}, respectively. Thus, the selectivity trend in the ternary metal ions system towards the $Z@Fe_3O_4$ NPs is observed to be $Cs^+ > Sr^{2+} > Co^{2+}$, which indicates that the competitive effect of Cs^+ is the strongest compared to Sr^{2+} and Co^{2+} ions.

Keywords: ternary metal ions; zeolite@magnetic nanoparticles ($Z@Fe_3O_4$NPs); adsorption kinetic; adsorption isotherm

Citation: Nguyen, T.V.; Nguyen, L.T.; Nguyen, H.T.T.; Le, T.-H. Adsorption Studies of Ternary Metal Ions (Cs^+, Sr^{2+}, and Co^{2+}) from Water Using Zeolite@Magnetic Nanoparticles ($Z@Fe_3O_4$ NPs). *Inorganics* **2024**, *12*, 276. https://doi.org/10.3390/inorganics12110276

Academic Editor: Aivaras Kareiva

Received: 29 July 2024
Revised: 5 September 2024
Accepted: 6 September 2024
Published: 25 October 2024

1. Introduction

A huge volume of radioactive liquid waste is frequently created during the performance of nuclear power plants, fuel recycling plants, hospitals, research institutes, and defense research institutes, which can cause potential environment. Also, radioactive waste can generate various negative health effects and is also the main cause of many dangerous diseases in humans, such as carcinoma of the liver, neurological disorders, liver cancer, kidney failure, and leukemia [1]. Thus, radioactive waste disposal is an urgent issue for the sustainable development of the nuclear, defense, and medical industries. Several methods, including ion exchange [2], membrane filtration [3], and adsorption [4,5], have been used to treat radioactive liquid waste to meet environmental discharge standards. Compared to these methods, inorganic adsorption by zeolite is attractive and promising for being more effective and economical due to its simplicity, selectivity, radiation stability, and good compatibility with the waste material [6]. In recent decades, many adsorption experiments used natural zeolites, synthetic zeolites, and a blend of the two for the decontamination of radioactive Cs and Sr [7,8]. However, the difficulty in separating the zeolite absorbent from the aqueous solution remains a drawback in this material. In the adsorption process,

magnetic separation is an optimal solution due to its advances in operation compared to filtration, centrifugation, or gravitational separation. Furthermore, magnetic iron oxide (Fe_3O_4) materials have attracted much attention in many environmental applications because Fe_3O_4 has good stability, high surface area, high co-effectivity, low toxicity, excellent magnetic responsivity, high dispersibility, and ease of surface modification [9–12]. Thus, zeolite could be engineered to become a magnetic material by loading Fe_3O_4 NPs onto the zeolite surface. Moreover, this material can also improve the surface area, resulting in increased adsorption capacity.

As we know, Cs, Sr, and Co are the most harmful radionuclides in radioactive waste. There are many studies on the reparation of a single radionuclide from waste solutions by inorganic sorbents [4–7,13,14], whereas few have considered the competitive adsorption of binary, ternary, or multiple radionuclides [15–17]. In addition, the metal ions in the aquatic environment interact with each other and compete to absorb into the adsorbent, which can influence the adsorption process. This is a challenge for removing multiple metal ions. Herein, zeolite@magnetic nanoparticles (Z@Fe_3O_4 NPs) were synthesized by loading magnetic nanoparticles (Fe_3O_4 NPs) onto the zeolite molecular sieve 4A surface using a precipitation method. Z@Fe_3O_4 NPs were applied as adsorbents for the removal of ternary metal ions (Cs^+, Sr^{2+}, and Co^{2+}) from water.

2. Results and Discussion

2.1. Characterizations of Z@Fe_3O_4 NPs

The field-emission scanning electron microscopy (FE-SEM) results in Figure 1a,b were analyzed to investigate the surface morphology of zeolite and Z@Fe_3O_4 NPs. The FE-SEM result of Z@Fe_3O_4 NPs exhibits that the spherical particle in the range of 25–50 nm has formed on the surface of the zeolite. Furthermore, the electron dispersive X-ray spectra (EDX) of Z@Fe_3O_4 NPs show the presence of Fe (Figure 1c), indicating that the loading of iron oxide nanoparticles onto the zeolite surface is successful. Meanwhile, X-ray diffraction (XRD) analysis exhibited a different crystal structure of Z@Fe_3O_4 NPs in comparison with the zeolite (Figure 1d). Before loading magnetic nanoparticles (Fe_3O_4 NPs), all diffraction peaks were assigned to zeolites [18].After loading magnetic nanoparticles (Fe_3O_4 NPs), the diffraction peaks were divided into two groups. The first group includes peaks at 2θ of 10.3, 12.7, 16.3, 21.8, 24.2, 27.3, 30.2, and 34.4°, which are assigned from zeolites, while the second group includes two diffraction peaks at 2θ of 35.5 and 62.6°, corresponding to the reflection of the (311) and (440) lattice planes, which can be indexed to the face-centered cubic structure of Fe_3O_4 according to JCPDS card No. 19-0629 [14,19].

The surface chemistry of Z@Fe_3O_4 NPs was characterized by X-ray photoelectron spectroscopy (XPS) (Figure 2a–c). A survey spectrum showed peaks corresponding to C 1s, O 1s, Si 2p, and Fe 2p, which demonstrated the existence of Fe on the zeolite surface (Figure 2a). As shown in Figure 2b, the Fe 2p exhibited two peaks at 712 and 724 eV, which corresponded to $Fe_{2p3/2}$ and $Fe_{2p1/2}$, respectively. Moreover, the high-resolution Fe $2p_{3/2}$ spectrum of Z@Fe_3O_4 NPs (Figure 2c) exhibited multi-component features that can be fitted by two Gaussian peaks at 710.0 and 711.8 eV, which can be indexed to Fe^{2+} and Fe^{3+}, respectively [20,21]. These indicate the successful formation of the Fe_3O_4 phase on the zeolite surface.

The formation of the Fe_3O_4 nanoparticle on the zeolite surface resulted in the enhancement of the nitrogen gas adsorption–desorption of Z@Fe_3O_4 NPs in comparison with zeolite 4A (Figure 2d). In addition, as shown in the surface area plot (Figure S1a,b), the surface area of the Z@Fe_3O_4 NPs (183.46 m^2/g) was higher than the zeolite (18.52 m^2/g). Therefore, the loading of Fe_3O_4 NPs onto the zeolite molecular sieve 4A surface not only makes it easy to separate Z@Fe_3O_4 NPs adsorbent from the solution using an external magnetic field, but also enhances the surface area. This will increase the Z@Fe_3O_4 NPs' ability to absorb metal ions.

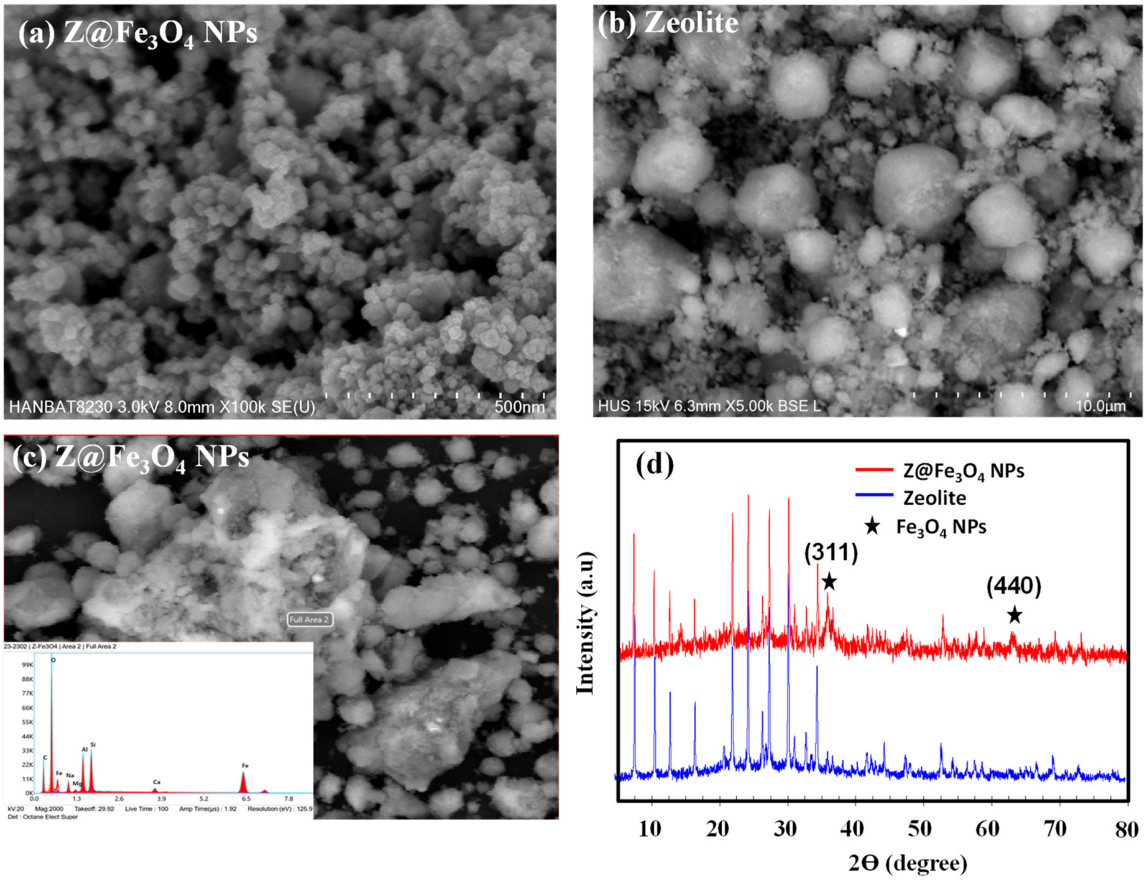

Figure 1. FE-SEM (**a**–**c**) and XRD (**d**) of Z@Fe_3O_4 NPs and zeolite.

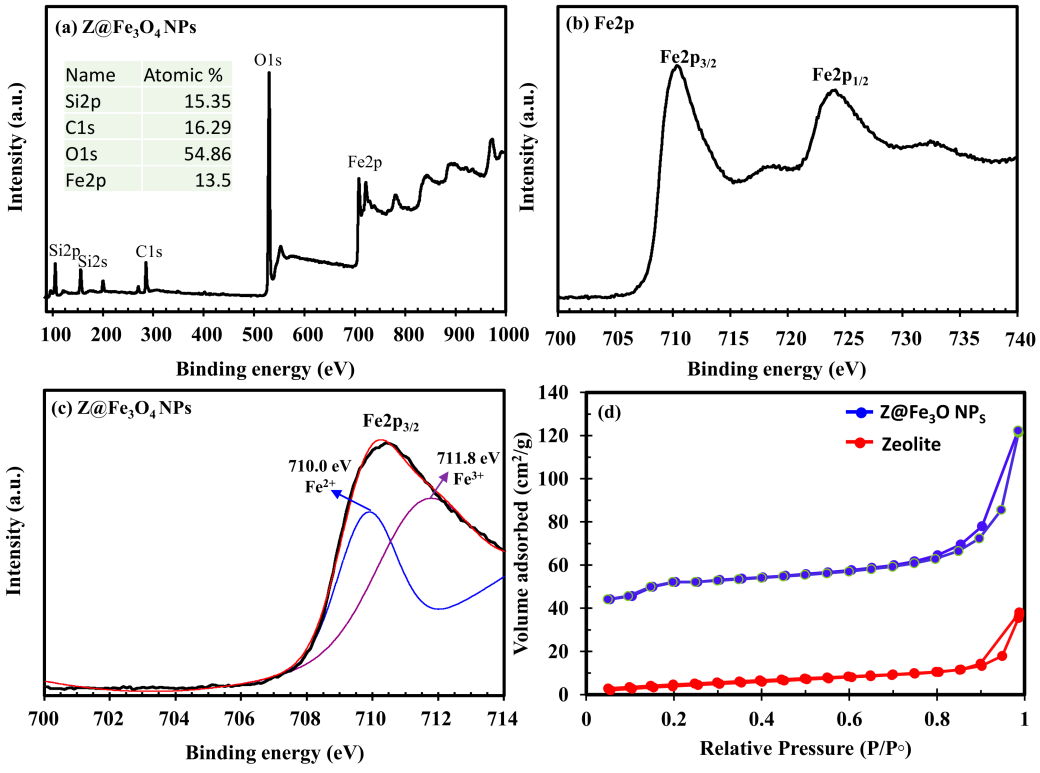

Figure 2. (**a**–**c**) XPS of Z@Fe_3O_4 NPs and (**d**) nitrogen gas adsorption–desorption isotherms of Z@Fe_3O_4 NPs and zeolite.

2.2. Adsorption Studies of Ternary Metal Ions Using Z@Fe_3O_4 NPs

2.2.1. Influence of the Adsorbent Weight and pH

The adsorbent weight is described as a significant parameter that influences the adsorption process. The adsorption process of ternary metal ions (Cs^+, Sr^{2+}, and Co^{2+}) from an aqueous solution is performed at diverse amounts of Z@Fe_3O_4 NPs in the range from 0.1 to 0.5 g at room temperature in the glove box. The pH, contact time, and initial concentration of ions are maintained at 6.9, 60 min, and 105 mg/L of each metal ion, respectively.

When the adsorbent weight rose from 0.1 to 0.5 g, the removal efficiency (R_e %) of each metal ion in a mixed solution (Cs^+, Sr^{2+}, and Co^{2+}) increased from 44.65 to 91.20%, 5.37 to 71.14%, and 0 to 47.14%, respectively. An enhancement in the removal efficiency along with an increase in the weight of Z@Fe_3O_4 NPs is due to the increase in the number of active adsorption sites and empty sites on the adsorbent surface (Figure 3). Although the enhancement amount of adsorbent provides additional active sites, the Z@Fe_3O_4 NPs adsorbent underwent agglomeration at high adsorbent concentrations, thereby decreasing the unoccupied adsorption active sites and effective surface area [22]. In addition, the initial concentration and volume of ternary metal ions (Cs^+, Sr^{2+}, and Co^{2+}) are constant, which results in the number of ions contacted and adsorbed by the adsorbent per unit mass decreasing with the increase in the adsorbent dose, and the active sites of the adsorbents are not saturated [23,24]. However, only the adsorption capacity of Cs^+ in mixed metal ions decreases from 46.89 to 19.15 mg/g as the adsorbent weight increases from 0.1 to 0.5 g. Contrarily, the adsorption capacity of Sr^{2+} and Co^{2+} in mixed metal ions initially increases in the adsorbent mass range (0.1–0.2 g) and reaches a maximum of 18.33 and 11.90 mg/g at 0.2 g, respectively, due to strong affinity of Z@Fe_3O_4 NPs with Cs^+. After that, the solid adsorption capacity of both ions then becomes almost constant as the adsorbent mass increases from 0.2 to 0.5 g. Because the adsorption capacity values of ternary metal ions (Cs^+, Sr^{2+}, Co^{2+}) were optimized at an adsorbent weight of 0.2 g, we chose the adsorbent weight of 0.2 g to survey the influencing factors.

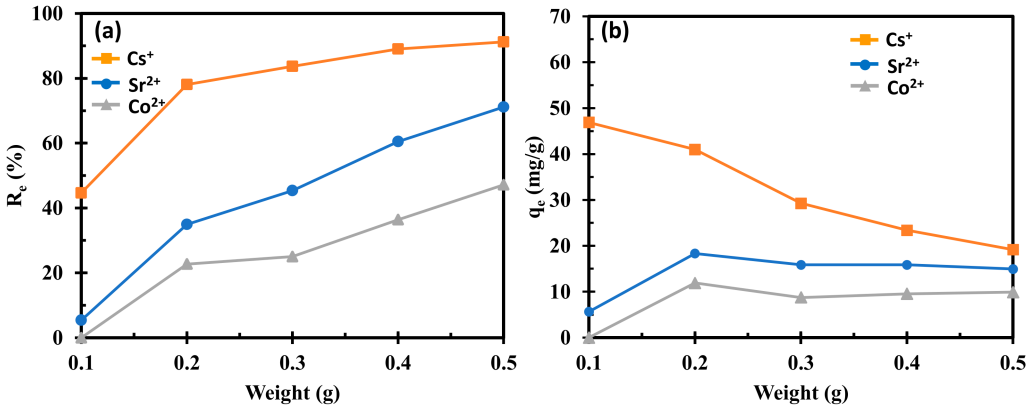

Figure 3. The influence of the adsorbent weight on the removal efficiency (R_e %) (**a**) and adsorption capacity (q_e) (**b**) of ternary metal ions from the aqueous solution.

The influence of the pH on the removal efficiency (Re%) and adsorption capacity (q_e) of ternary metal ions (Cs^+, Sr^{2+}, and Co^{2+}) from the aqueous solution are performed at a pH from 3.0 to 10.0 and at room temperature (Figure 4a,b). HCl 0.1 M and NaOH 0.1 M were added to the adsorption system to adjust the pH values of the solution ranging from 3 to 10. The initial concentration of ions, adsorbent mass, and contact time are maintained at 105 mg/L of each metal ion, 0.2 g, and 60 min, respectively. Figure 4 depicts that the removal efficiency and adsorption capacity of three ions slightly increased as the pH solution increased from 3.0 to 8.0. Subsequently, it showed that the removal efficiency and adsorption capacity of Cs^+ ions decreased, while $Sr^{2+}$and Co^{2+} ions exhibited a rapid increase and their removal efficiency and adsorption capacity were higher than Cs^+. As we

know, the pH of the aqueous solution was a critical parameter for the absorption of metal ions experiments because it affected the surface charge of the adsorbent as well as the metal ion chemistry structure in the solution [25–28]. The surface charge of the adsorbent depends on their zero-point charge (Zpc) [27,28]. When the pH of the solution is above the Zpc value, the adsorbent surface becomes more negatively charged. On the contrary, the surface charge of the adsorbent is more positive as the pH is lower than Zpc. Furthermore, the Zpc value depends on the nature of the nanoparticle [25,26]. According to previous works, the Zpc values of the magnetic materials vary between 4.0 and 6.5 [28–33]. Meanwhile, Belachew et al. reported that the Zpc of the zeolite 4A was determined to be 6.8 [34]. Since the Z@Fe_3O_4 NPs adsorbent was synthesized by loading Fe_3O_4 NPs onto the zeolite 4A surface using a precipitation method, we suggested that the zero-point charge (Zpc) of the Z@Fe_3O_4 NPs adsorbent is between 4.0 and 7.0. In addition to affecting the surface charge of the adsorbent material, the pH value also affects the metal ion chemistry structure in the solution, resulting in changes in the charge and size of the metal ions [26–29]. Ali et al. observed the distributions of Cs, Sr, and Co species (C = 100 mg/L) as a function of pH [35]. The authors indicated that the metal ion chemistry structure of Cs in the solution was the dominant Cs+ ion at a pH ranging from 1.0 to 12.0. Meanwhile, the metal ion chemistry structure of Sr was the dominant Sr^{2+} ion at a pH ranging from 1.0 to 8.0 and was the $Sr(OH)^+$ ion at a pH above 8.0 [35]. For Co, the metal ion chemistry structure was the dominant Co^{2+} ion at a pH ranging from 1.0 to 8.0 and was $Co(OH)_2$ at a pH above 8.0 [12,35]. Thus, we propose that when the pH solution increases from 3.0 to 8.0, the surface charge of Z@Fe_3O_4 NPs becomes gradually negative, while the metal ions' chemistry structure in the solution is the dominant species of cation. These lead to the gradual enhancement of the electrostatic attraction between the positive charge on the adsorbent surface and cations, the removal efficiency, and the adsorption capacity of ternary metal ions (Cs^+, Sr^{2+}, and Co^{2+}). However, there is no significant increase in the removal efficiency and adsorption capacity. Table S2 shows the pH of the solution after adsorption increases as compared to before adsorption at a pH ranging from 3.0 to 7.0. This indicates that competition between H^+ ions and three metal ions for the adsorption on Z@Fe_3O_4 NPs occurs, which makes the removal efficiency and adsorption capacity of the three ions see no significant increase.

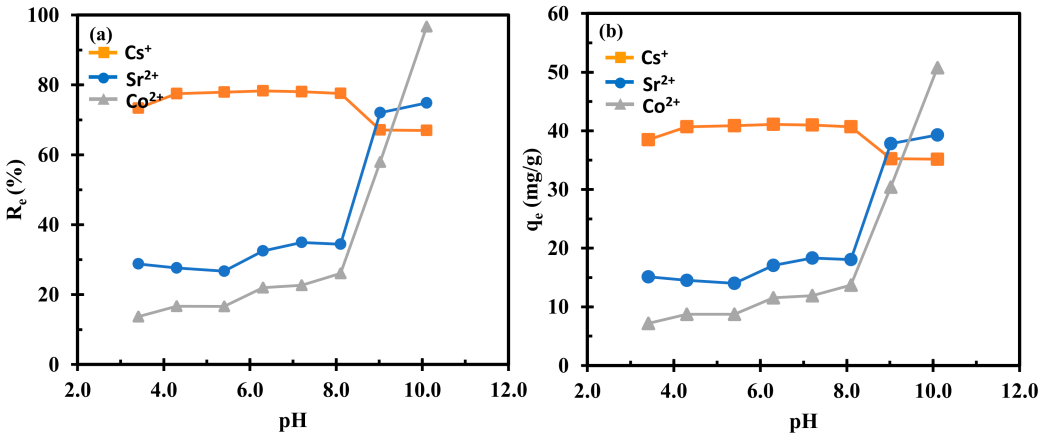

Figure 4. Effect of pH on removal efficiency (Re%) (**a**) and adsorption capacity (q_e) (**b**) of ternary metal ions (Cs^+, Sr^{2+}, and Co^{2+}).

In addition, it was found that the removal efficiency and adsorption capacity of Cs^+ in mixed metal ions decreased at a pH above 8.0, while $Sr^{2+}$and Co^{2+}showed rapid increases, with their removal efficiency and adsorption capacity being higher than Cs^+. Because the Cs and Sr exist mainly in the form of Cs^+ and $Sr(OH)^+$ at pH values above 8.0 [27,35], the radius of the $Sr(OH)^+$ ion (260 pm) is higher than the Cs^+ion (186 pm) [36]. This result leads to $Sr(OH)^+$ ions having higher binding power and higher adsorption than Cs^+ ions [14,35].

For Co^{2+} ions, the strong increase in the removal efficiency and adsorption capacity at pH values above 8.0 is due to the formation of hydroxide precipitation [12,35]. Therefore, a part of Co^{2+} ion removal is due to the formation of $Co(OH)_2$ precipitation at a pH above 8. For this reason, the next absorption experiment should be carried out at a pH range of 6.0–7.0.

Furthermore, Figure 4a,b exhibit q_e values of ternary metal ions following the order Cs+ > Sr^{2+} > Co^{2+}. This indicates that there is competitive absorption for mixtures of metal ions onto Z@Fe_3O_4 NPs. The competitive adsorption of Cs^+, Sr^{2+}, and Co^{2+} ions onto Z@Fe_3O_4 NPs depends on how these metal ions interact with the adsorbent. In addition, the interaction between Cs^+, Sr^{2+}, and Co^{2+}ions and Z@Fe_3O_4 NPs depends on the metal's molecular mass, ion charges, ionic radius, hydration energy, and electrostatic charge [37,38]. The difference in the radius of metal ions has a significant influence on the absorption capacity; ions with a smaller radius have high mobility in aqueous solutions, and thus, they have a lower tendency to absorb onto magnetic nanoparticle adsorbents [35]. Moreover, the order of the ionic radii of three ions is as follows: Cs^+ (186 pm) > Sr^{2+} (132 pm) > Co^{2+} (79 pm) [27]. Hence, the Cs^+ ion with the highest ionic radius has the highest binding power and highest adsorption onto Z@Fe_3O_4 NPs as compared to Sr^{2+} and Co^{2+} ions at pH values below 8. This result reveals that Z@Fe_3O_4 NPs behaved more selectively toward Cs^+ ions at pH values below 8. However, it has been found that the order adsorption capacity of ternary metal ions changed (such as Sr^{2+} > Cs^+) as pH values reached above 8. As we discussed above, the interaction between metal ions and Z@Fe_3O_4 NPs was affected by the ionic radius. Furthermore, Cs and Sr exist mainly in the form of Cs^+ and $Sr(OH)^+$ at pH values above 8.0, which results in the radius of the $Sr(OH)^+$ ion (260 pm) being higher than Cs^+ (186 pm) [36]. Thus, the $Sr(OH)^+$ ions with higher ionic radii resulted in higher binding powers and higher adsorptions as compared to Cs^+ with pH values above 8.0.

2.2.2. A Study on Adsorption Kinetic

One of the important factors that affect the adsorption process of ternary metal ions is the contact time. The effect of the contact time on the adsorption capacity (q_e) of ternary metal ions (Cs^+, Sr^{2+}, and Co^{2+}) from aqueous solutions is performed at a contact time range from 5 to 180 min and at room temperature. The pH, initial concentration of each ion, and the adsorbent mass are maintained at 6.3, 105 mg/L (each metal ion), and 0.2 g, respectively. Table S3 and Figure S2a clearly show that with an increase in the contact time, the adsorption capacity of all studied metal ions gradually increased until reaching equilibrium at 50 min. Therefore, the contact time of 60 min is an ideal time to investigate the effect of other factors on the adsorption of ternary metal ions (Co^{2+}, Sr^{2+}, and Cs^+).

Kinetic adsorption models illustrate the mechanism of adsorption of metal ions and particularly determine the rate of removal of metals ion from the aqueous medium, which will provide the optimized design parameters such as the adsorbate residence time and kinetic rate constant. In this study, Pseudo-first-order, Pseudo-second-order, Intra-particle diffusion kinetic, and Elovich models were used to simulate the absorption kinetics of ternary ion adsorption (Cs^+, Sr^{2+}, and Co^{2+}) onto Z@Fe_3O_4 NPs. Four kinetic models have been investigated as follows [39]:

Pseudo-first-order equation:

$$\ln(q_e - q) = \ln(q_e) - k_1 t \quad (1)$$

Pseudo-second-order equation:

$$\frac{1}{q} = \left(\frac{1}{q_e}\right)t + \left(\frac{1}{k_2 \times {q_e}^2}\right) \quad (2)$$

Elovich equation:

$$q = \frac{\ln a_e b_e}{b_e} + \frac{1}{b_e}\ln t \quad (3)$$

Intra-particle diffusion equation:

$$q = k_{int} t^{0.5} \quad (4)$$

where q_e (mg/g) is the amount of metal ions at equilibrium; k_1 (min^{-1}) is the kinetic rate constant for the Pseudo-first-order model calculated by a linear plot of ln ($q_e - q$) against time; k_2 (g/mg·min) is the equilibrium rate constant for the Pseudo-second-order model obtained from the intercept of the linear plot of t/q against t; a_e (mg/g·min) is the initial sorption rate; b_e (g/mg) is the constant related to the surface coverage and activation energy of chemisorption in the Elovich mode; and k_{int} (mg/g·$min^{0.5}$) is the Intra-particle diffusion rate constant calculated from the slope of the plot q versus $t^{0.5}$.

From Figure 5a and Table 1, the experimental adsorption data showed a good fit to the Pseudo-first-order model with correlation coefficient (R^2) values of 0.9415 for Sr^{2+} and 0.9573 for Co^{2+}. In Cs^+ adsorption, the model did not fit well with the experimental result with a low R^2 value of 0.4622. Moreover, the calculated equilibrium capacities (q_e) obtained from the analysis of Cs^+ (4.43 mg/g), Sr^{2+} (10.00 mg/g), and Co^{2+} (8.58 mg/g) were lower than the experimental values for Cs^+ (43.29 mg/g), Sr^{2+} (20.46 mg/g), and Co^{2+} (14.70 mg/g). These results suggested that the pseudo-first-order model might not be applicable for the adsorption of ternary ion adsorption (Cs^+, Sr^{2+}, and Co^{2+}) onto $Z@Fe_3O_4$ NPs.

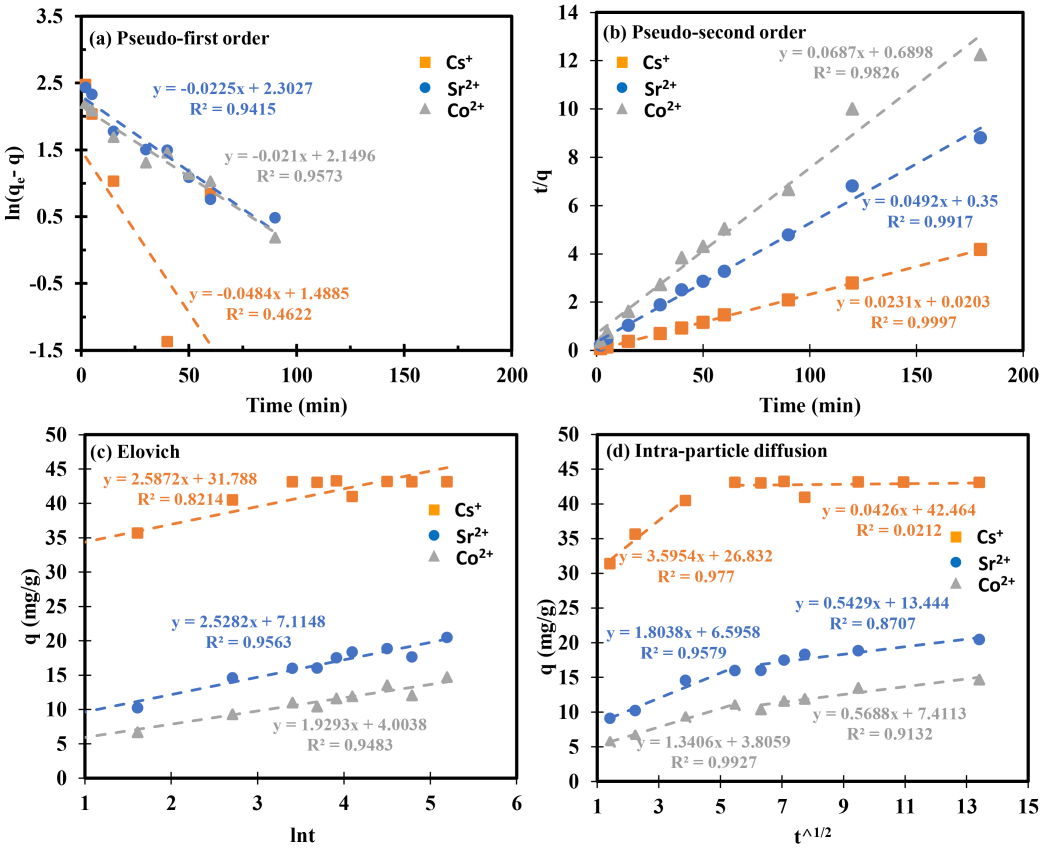

Figure 5. The linear regression analysis of kinetic models ((**a**) Pseudo-first-order, (**b**) Pseudo-second-order, (**c**) Elovich models, and (**d**) Intra-particle diffusion) of ternary metal ions on $Z@Fe_3O_4$ NPs.

The Pseudo-second-order kinetic model was also applied for the adsorption kinetics of ternary metal ion adsorption. The calculated amount of three metal ions at equilibrium (q_e) was in the following order: $Co^{2+} < Sr^{2+} < Cs^+$. This result confirms that the $Z@Fe_3O_4$ NPs adsorbent has a stronger affinity for Cs^+ than Sr^{2+} and Co^{2+}ions.Furthermore; the correlation coefficient (R^2) of three metal ions has the highest values and is closest to unity as compared to the other three models, which indicates that the pseudo-second-order

kinetic model provides almost a perfect fit to the experimental data. In addition, the q_e of Cs^+ (43.29 mg/g), Sr^{2+} (20.33 mg/g), and Co^{2+} (14.56 mg/g) values obtained from the slope of the plot of t/q versus t were the closest to the experimental data (Table 2). Hence, we assumed that the adsorption of ternary ions onto Z@Fe_3O_4 NPs was a chemisorption process.

Table 1. The parameters of kinetic absorption for ternary metal ions on Z@Fe_3O_4 NPs.

Kinetic Adsorption Parameters		Ternary Ions Absorption		
		Cs^+	Sr^{2+}	Co^{2+}
Pseudo-first-order	$q_{e.exp}$(mg/g)	43.29	20.46	14.70
	$q_{e\cdot cal}$ (mg/g)	4.43	10.00	8.58
	k_1 (min^{-1})	0.048	0.023	0.021
	R^2	0.4622	0.9415	0.9573
Pseudo-second-order	$q_{e\cdot cal}$(mg/g)	43.29	20.33	14.56
	k_2 (g/mg·min)	0.026	0.007	0.007
	R^2	0.9997	0.9917	0.9826
Elovich	a_e (mg/g·min)	5.61×10^5	4.22×10^1	1.54×10^1
	b_e (g/mg)	3.87×10^{-1}	3.96×10^{-1}	5.18×10^{-1}
	R^2	0.8214	0.9563	0.9483
Intra-particle diffusion	k_{int1}(mg/g·$min^{0.5}$)	3.59	1.80	1.34
	R^2_1	0.9770	0.9579	0.9927
	k_{int2}(mg/g·$min^{0.5}$)	0.042	0.542	0.568
	R^2_2	0.0212	0.8707	0.9132

$q_{e\cdot exp}$: experimental equilibrium capacity; $q_{e\cdot cal}$: calculated equilibrium capacity.

Table 2. The relative parameters of the adsorption isotherms for ternary ions on Z@Fe_3O_4 NPs.

Kinetic Adsorption Parameters		Ternary Ions Absorption		
		Cs^+	Sr^{2+}	Co^{2+}
Dubinin–Radushkevich isotherm	q_{max} (mg/g)	26.95	13.17	9.77
	β(mol^2/J^2)	4.0×10^{-7}	7.0×10^{-8}	1.0×10^{-7}
	E (kJ/mol)	1.12	2.67	2.24
	R^2	0.7959	0.8168	0.6676
Temkin isotherm	δ_T (kJ/mol)	0.24	1.46	2.23
	K_T (L/g)	2.15	149.51	251.56
	R^2	0.9546	0.6829	0.5583
Freundlich isotherm	n_F	1.70	5.43	6.89
	K_F (mg/g)	8.23	7.70	5.94
	R^2	0.8908	0.7408	0.6477
Langmuir isotherm	q_{max}(mg/g)	48.31	15.02	10.41
	K_L (L/mg)	0.19	2.07	0.69
	R^2	0.9758	0.9206	0.9441

q_{max}: calculated maximum capacity.

The Elovich model was applied to further characterize the assumption of chemisorption for the heterogeneous system. As seen in Table 1 and Figure 5c, the initial adsorption rate (a_e) of three metal ions was in the following order: $Cs^+ > Sr^{2+} > Co^{2+}$. Meanwhile, the

constant related to the surface coverage and activation energy of chemisorption (b_e) was in the following reverse order: $Co^{2+} > Sr^{2+} > Cs^{+}$. However, in Cs^{+} adsorption, the model also did not fit well with the experimental result with a low R^2 value of 0.8555. Whereas, a good fit of Sr^{2+} and Co^{2+} adsorption data was obtained with a higher R^2 value (0.9563 and 0.9483). Thus, the Elovich model suggests that chemisorption might be significantly involved in Sr^{2+} and Co^{2+}, but not in Cs^{+} adsorption onto Z@Fe_3O_4 NPs.

The Intra-particle diffusion adsorption kinetic model is one of the most widely applied for the adsorption kinetics of metal ions. The plot of q_t versus $t^{1/2}$ (Figure 5d) for ternary ion adsorption (Cs^{+}, Sr^{2+}, and Co^{2+}) onto Z@Fe_3O_4 NPs demonstrated multi-linear plots. In the first plots, the high slopes indicated the high diffusion rate constant values (k_{int1}) of three metal ions, which was due to the availability of a massive number of active sites on the Z@Fe_3O_4 NPs surface [40]. It means that this first step is instantaneous adsorption or external surface adsorption [40]. In the second plot, the low slopes indicated the low diffusion rate constants (k_{int2}), which are due to a decrease in the concentration gradient [40]. In addition, the diffusion rate constants (k_{int2}) of Cs^{+}, Sr^{2+}, and Co^{2+}ions into the mesopores of the Z@Fe_3O_4 NPs were lower than the first step. These suggested that the second step was the progressive adsorption or intra-particle diffusion stage [40]. On the other hand, a good fit of three metal ion adsorption data at the first step was obtained with higher R^2 values of 0.9770, 0.9579, and 0.9927, respectively. Nevertheless, this model did not fit well at the second step of adsorption with a low R^2 value of 0.0212 for Cs^{+} and 0.8707 for Sr^{2+}, respectively, while a good fit of Co^{2+}adsorption data at the second step was obtained with a high R^2 value of 0.9132. These results indicate that the intra-particle diffusion model might not be applicable for Cs^{+} and Sr^{2+}, but is significantly involved in Co^{2+} adsorption onto Z@Fe_3O_4 NPs.

2.2.3. A Study on Absorption Isotherms

The initial concentration was also one of the important factors that affected the adsorption process. The effect of the initial concentration on the adsorption capacity (q_e) of ternary metal ions from an aqueous solution has been characterized by using 0.2 g of Z@Fe_3O_4 NPs with 100 mL of a mixed metal ion solution with different initial concentrations (from 10 to 150 mg/L). The pH and the contact time are maintained at 6.2 for 60 min under room temperature with stirring. Figure S2b and Table S4 showed that with a rise in the initial concentration of ternary metal ions, the adsorption capacity of three ions enhanced rapidly until reaching a maximum at 105 mg/L for Cs^{+} and 80 mg/L for Sr^{2+} and Co^{2+}. After that, the adsorption capacity of all three ions decreased as the initial concentration increased from 80 to 150 mg/L. This observation could be attributed to the ratio between the active sites of the Z@Fe_3O_4 NPs adsorbent and the fact that the number of moles of ions was huge at a low initial metal ion concentration range (10 to 105 mg/L). Nevertheless, the ratio between the number of moles of ions and the active sites of the Z@Fe_3O_4 NPs adsorbent decreased as the initial concentration of ions enhanced over 105 mg/L; this was because the available number of moles of metal ions is still enhanced, while the active sites of the Z@Fe_3O_4 NPs are constant. This leads to a decrease in the adsorption capacity of the Z@Fe_3O_4 NPs adsorbent.

Dubinin–Radushkevich (D–R), Temkin, Langmuir, and Freundlich isotherm models were applied to simulate the adsorption mechanism of ternary metal ions onto the Z@Fe_3O_4 NPs surface. Four isotherm models have been investigated as follows:

Dubinin–Radushkevich model [41]:

$$\ln q_e = \ln q_{max} - \beta \varepsilon^2 \quad (5)$$

Temkin model [42]:

$$q_e = \frac{RT}{\delta_T} \ln K_T + \frac{RT}{\delta_T} \ln C_e \quad (6)$$

Freundlich model [43]:

$$\ln q_e = \ln K_F + \frac{1}{n_F} \ln C_e \quad (7)$$

Langmuir model [43]:

$$\frac{1}{q_e} = \frac{1}{q_{max} K_L C_e} + \frac{1}{q_{max}} \quad (8)$$

where β (mol^2/J^2) is a constant related to the adsorption energy, q_{max} (mg/g) is the maximum capacity of the adsorbent, and ε ($kJ \cdot mol^{-1}$) is the adsorption potential. The adsorption potential ε (kJ/mol) is calculated using Equation (15):

$$\varepsilon = RT \ln\left(1 + \frac{1}{C_e}\right) \quad (9)$$

The parameter β could be used to estimate the mean free energy E (kJ/mol) using the following equation:

$$E = \frac{10^{-3}}{\sqrt{2\beta}} \quad (10)$$

K_T (L/g) is the Temkin isotherm equilibrium binding constant; δ_T (kJ/mol) is the Temkin isotherm constant; R is the universal gas constant (8.314 J/mol·K); and T is the temperature at 298K. K_F (mg/g) is the Freundlich isotherm constant, n_F is the adsorption intensity, and C_e is the equilibrium concentration of Cs^+, Sr^{2+}, and Co^{2+} ions (mg/L). K_L (L/mg) is the Langmuir isotherm constant and q_{max}(mg/g)is the maximum monolayer coverage capacity. The vital features of the Langmuir isotherm can be described by a separation factor R_L. The separation factor or equilibrium parameter R_L is a dimensionless constant, which is defined by the following equation [41]:

$$R_L = 1/(1 + K_L C_0) \quad (11)$$

The R_L value assumes the nature and the feasibility of the adsorption process, such as linear ($R_L = 1$), irreversible ($R_L = 0$), unfavorable ($R_L > 1$), or favorable ($0 < R_L < 1$).

Figure 6 and Table 2 illustrate the resulting plots of the Dubinin–Radushkevich, Temkin, Freundlich, and Langmuir isotherm models of ternary metal ions (Cs^+, Sr^{2+}, and Co^{2+}ions) onto the surface of Z@Fe_3O_4 NPs. The Langmuir isotherm model was found to be the best model (with R^2 values higher than 0.9206) to describe the ternary metal ion absorption by Z@Fe_3O_4 NPs. This indicates that the ternary metal ion adsorption process is characterized by monolayer adsorption. The ternary metal ions absorption by Z@Fe_3O_4 NPs was based on the electrostatic attraction. Furthermore, the important characteristics of the Langmuir isotherm can be described by a separation factor R_L, which was obtained in the range from 0 to 1 (Figure S3). This indicates that the adsorption of ternary metal ions by Z@Fe_3O_4 NPs is favorable. Furthermore, the maximum monolayer coverage capacities (q_{max}) for three ions follow the order of Cs^+ (48.31 mg/g) > Co^{2+} (15.02 mg/g) > Sr^{2+} (10.41 mg/g), which is the same as their ionic radius sequence. The Cs^+ (186 pm) ion has the highest ionic radius as compared to Co^{2+} and Sr^{2+}, resulting in higher binding power and higher adsorption. Thus, Z@Fe_3O_4 NPs behaved more selectively toward Cs^+ ions in the competitive adsorption of ternary metal ion systems (Cs^+, Sr^{2+}, and Co^{2+} ions).

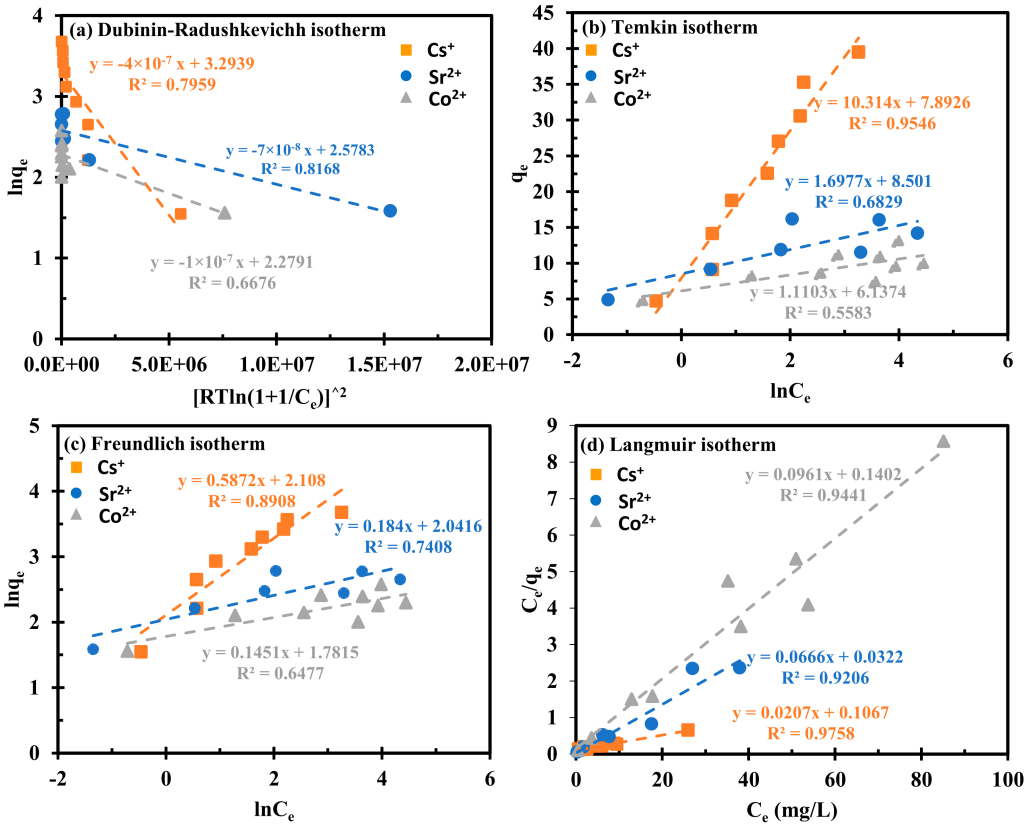

Figure 6. The linear regression analysis of adsorption isotherm models of ternary metal ions on Z@Fe_3O_4 NPs: (**a**) Dubinin–Radushkevich; (**b**) Temkin; (**c**) Freundlich; and (**d**) Langmuir isotherm models).

3. Materials and Methods

3.1. Chemical and Materials

In this work, iron (II) chloride tetrahydrate ($FeCl_2 \cdot 4H_2O$, 99%), calcium hydroxide ($Ca(OH)_2$, 99%), cobalt (II) sulfate heptahydrate ($CoSO_4 \cdot 7H_2O$, >99%), hydrochloric acid (HCl, 36%), strontium chloride ($SrCl_2$, 99%), sodium hydroxide (NaOH, 99%), ethanol (C_2H_5OH, 99.5%), and cesium chloride (CsCl, 99%) were provided from Merck, Darmstadt, Germany. The zeolite molecular sieve 4A was purchased from Guangdong Xintao Technology Co., Ltd. Zhuhai City, Guangdong province, China. Before the synthesis of zeolite@magnetic nanoparticles (Z@Fe_3O_4 NPs), the zeolite molecular sieve 4A was carefully crushed and sieved to an 80 mesh particle size.

3.2. Synthesis of Zeolite@Magnetic Nanoparticles (Z@Fe_3O_4 NPs)

The zeolite@magnetic nanoparticles (Z@Fe_3O_4 NPs) were synthesized by loading magnetic nanoparticles (Fe_3O_4 NPs) onto the zeolite molecular sieve 4A surface using a precipitation method, as shown in Scheme 1 [9,44]. Firstly, 1 g zeolite was mixed with 100 mL saturated $Ca(OH)_2$ solution by stirring for 30 min. $FeCl_2$ 2.4 M was then added dropwise into the as-prepared suspension with a stirring speed of 700 rpm until the pH of the mixture about 7~8. The reaction mixture was stirred for 30 min at room temperature. After the reaction time was completed, the brown precipitate was separated from the reaction mixture by centrifugation at 10,000 rpm for 5 min. The precipitate was washed with distilled water (three times) and ethanol (three times). To remove water and ethanol, the solid sample was dried at 50 °C in a vacuum oven for 24 h. Finally, we obtained

brown powder (Z@Fe_3O_4 NPs). The reaction mechanism that occurs during the synthesis of Z@Fe_3O_4 NPs is shown through the equations below [9,14]:

$$Ca(OH)_2 + FeCl_2 \rightarrow CaCl_2 + Fe(OH)_2 \quad (12)$$

$$1/2O_2 + Fe(OH)_2 \rightarrow Fe_2O_3 + 2H_2O \quad (13)$$

$$Fe(OH)_2 \rightarrow FeO + H_2O \quad (14)$$

$$FeO + Fe_2O_3 \rightarrow Fe_3O_4 \quad (15)$$

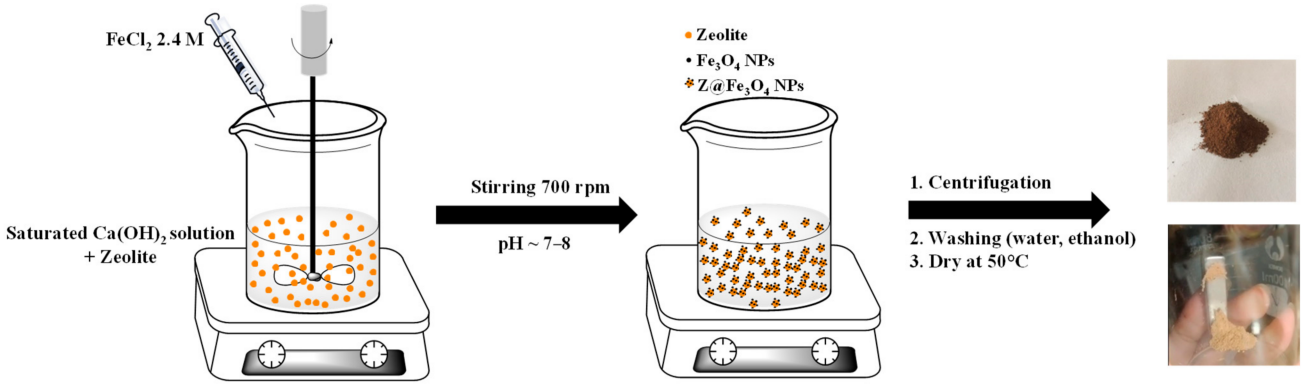

Scheme 1. Synthesis procedure of zeolite@magnetic nanoparticles (Z@Fe_3O_4 NPs).

Field-emission scanning electron microscope (FE-SEM) using a Regulus 8230 (Hitachi, Tokyo, Japan) and energy dispersive X-ray (EDX) analyses were performed to investigate the microstructure of the Z@Fe_3O_4 NPs and zeolite. For analyzing a Z@Fe_3O_4 NPs' surface chemistry, X-ray photoelectron spectroscopy (XPS) was applied using a Thermo Scientific K-Alpha (Manchester, UK) with an Al Kα(1486.6 eV) source at a pass energy of 1–400 eV. The crystal structure of Z@Fe_3O_4 NPs and zeolite was determined by X-ray diffraction (XRD) spectra using D8 Discover, Bruker, Karlsruhe, Germany. Nitrogen (N_2) adsorption–desorption isotherms of Z@Fe_3O_4 NPs and zeolite at 77K were analyzed with Quantachrome mod. NOVA 2200e, Boynton Beach, FL, USA. The specific surface area of Z@Fe_3O_4 NPs and zeolite were typically determined by using the Brunauer–Emmett–Teller (BET) analysis. The concentration of Cs^+, Sr^{2+}, and Co^{2+} ions in the aqueous solution was analyzed by inductively coupled plasma–mass spectrometry (plasma Agilent 8900 Triple Quadrupole ICP-MS, Santa Clara, CA, USA).

3.3. Adsorption Experiments

The adsorption of ternary metal ions (Cs^+, Sr^{2+}, and Co^{2+}) onto Z@Fe_3O_4 NPs has been studied by using batch-adsorption techniques. The absorption properties of Z@Fe_3O_4 NPs for ternary metal ions were investigated by changing the effective factors, such as the adsorbent weight (0.1 to 0.5 g), pH (3 to 10), contact time (5 to 180 min), and initial concentration of ions (10 to 150 mg/L). The detailed experiment of the adsorption of ternary metal ions from water using Z@Fe_3O_4 NPs was explained and summarized in the supporting information. The Cs^+, Sr^{2+}, and Co^{2+} concentrations in the aqueous solution after the adsorption process were analyzed by ICP-MS spectrometry. The removal efficiency (R_e%) and adsorption capacity (q_e) was calculated by Equations (5) and (6) as follows [11]:

$$Re\% = \frac{C_0 - C_e}{C_0} \times 100(\%) \quad (16)$$

$$q_e = \frac{V_0(C_0 - C_e)}{m} \quad (17)$$

where C_0 and C_e are the initial and equilibrium concentrations of the metal ions, respectively (mg/L); V_0 is the volume of the aqueous phase (L); and m is the adsorbent mass (g).

4. Conclusions

In this work, the zeolite@magnetic nanoparticles (Z@Fe_3O_4 NPs) were successfully synthesized to remove ternary metal ions (ternary metal ion systems), including Cs^+, Sr^{2+}, and Co^{2+} ions, from water. In particular, loading Fe_3O_4 NPs onto the zeolite molecular sieve 4A surface not only easily separates the Z@Fe_3O_4 NPs adsorbent from the solution using an external magnetic field, but also enhances the surface area, leading to an increase in the Z@Fe_3O_4 NPs' ability to absorb metal ions. These adsorption results revealed that the ternary metal ion adsorption is dependent on the adsorbent mass, solution pH, contact time, and initial metal ion concentration. The optimized condition for the removal of ternary metal ions is obtained at the adsorbent mass of 0.2, pH of 6.0~7.0, and contact time of 60 min. In kinetics studies, the kinetic adsorption of ternary metal ion systems fitted well to the pseudo-second-order model. Thus, the adsorption of ternary ions onto Z@Fe_3O_4 NPs was a chemisorption process. Furthermore, based on the isotherm adsorption investigations of the ternary metal ion system, it shows that the Langmuir isotherm model was found to be the best model (with R^2 values higher than 0.9206) to describe the ternary metal ion absorption by Z@Fe_3O_4 NPs. This indicates that the ternary metal ion adsorption process is characterized by monolayer adsorption. Furthermore, the maximum adsorption capacities of Cs^+, Sr^{2+}, and Co^{2+}obtained from the Langmuir model are 48.31, 15.02, and 10.41 mg/g, respectively. Thus, the selectivity trend in the ternary metal ion system towards the Z@Fe_3O_4 NPs is observed to be $Cs^+ > Sr^{2+} > Co^{2+}$, which indicated that the competitive effect of Cs^+ was the strongest.

Supplementary Materials: The following supporting information can be downloaded at https://www.mdpi.com/article/10.3390/inorganics12110276/s1, Figure S1: Surface area plot of Z@Fe3O4 NPs (a) and zeolite (b); Table S1: Effect of the adsorbent weight. Table S2: Effect of pH; Table S3: Effect of the contact time; Table S4: Effect of the initial concentration of metal ions; Figure S2: Effect of the contact time (a) and initial concentration of metal ions (b) on the adsorption capacity (q_e) of ternary metal ions (Cs+, Sr^{2+}, and Co^{2+}) from aqueous solution; Figure S3: The dependence of the separation factor RL values on the initial concentrations of three metal ions C_0.

Author Contributions: Conceptualization, T.V.N. and T.-H.L.; methodology, H.T.T.N.; formal analysis, L.T.N.; investigation, H.T.T.N., T.V.N. and T.-H.L.; data curation, T.V.N. and T.-H.L.; writing—original draft preparation, T.V.N. and T.-H.L.; writing—review and editing, T.V.N. and T.-H.L.; visualization, T.-H.L.; supervision, T.-H.L. All authors have read and agreed to the published version of the manuscript.

Funding: This research received no external funding.

Data Availability Statement: The data that support the plots within this paper are available from the corresponding author upon reasonable request.

Acknowledgments: We would like to thank Thuyloi University and Institute for Technology of Radioactive and Rare Elements, Viet Nam for the support of time and facilities for this study.

Conflicts of Interest: The authors declare no competing financial interest.

References

1. Jiseon, J.; Lee, D.S. Magnetic Prussian blue nanocomposites for effective cesium removal from aqueous solution. *Ind. Eng. Chem. Res.* **2016**, *55*, 3852–3860.
2. Hassan, N.M.; Adu-Wusu, K. Cesium removal from hanford tank waste solution using resorcinol-formaldehyde resin. *Solvent Extr. Ion Exch.* **2005**, *23*, 375–389. [CrossRef]
3. Liu, H.; Wang, J. Treatment of radioactive wastewater using direct contact membrane distillation. *J. Hazard. Mater.* **2013**, *261*, 307–315. [CrossRef]
4. Repo, E.; Malinen, L.; Koivula, R.; Harjula, R.; Sillanpää, M. Capture of Co(II) from its aqueous EDTA-chelate by DTPA-modified silica gel and chitosan. *J. Hazard. Mater.* **2011**, *187*, 122–132. [CrossRef] [PubMed]

5. Nilchi, A.; Hadjmohammadi, M.R.; Garmarodi, S.R.; Saberi, R. Studies on the adsorption behaviour of trace amounts of $90Sr^{2+}$, $140La^{3+}$, $60Co^{2+}$, Ni^{2+} and Zr^{4+} cations on synthesized inorganic ion exchangers. *J. Hazard. Mater.* **2009**, *167*, 531–535. [CrossRef]
6. Kong, S.; Wang, Y.; Zhan, H.; Yuan, S.; Yu, M.; Liu, M. Adsorption/oxidation of arsenic in groundwater by nanoscale Fe-Mn binary oxides loaded on zeolite. *Water Environ. Res.* **2014**, *86*, 147–155. [CrossRef]
7. Munthali, M.W.; Johan, E.; Aono, H.; Matsue, N. Cs^{+} and Sr^{2+} adsorption selectivity of zeolites in relation to radioactive decontamination. *J. Asian Ceram. Soc.* **2015**, *3*, 245–250. [CrossRef]
8. Osmanlioglu, A.E. Treatment of radioactive liquid waste by sorption on natural zeolite in Turkey. *J. Hazard. Mater.* **2006**, *137*, 332–335. [CrossRef]
9. Singh, A.K.; Srivastava, O.N.; Singh, K. Shape and size-dependent magnetic properties of Fe_3O_4 nanoparticles synthesized using piperidine. *Nanoscale Res. Lett.* **2017**, *12*, 298. [CrossRef]
10. da Costa, G.; De Grave, E.; de Bakker, P.; Vandenberghe, R. Synthesis and characterization of some iron oxides by Sol-Gel method. *J. Solid State Chem.* **1994**, *113*, 405–412. [CrossRef]
11. Zargoosh, K.; Abedini, H.; Abdolmaleki, A.; Molavian, M.R. Effective Removal of Heavy Metal Ions from Industrial Wastes Using Thiosalicylhydrazide-Modified Magnetic Nanoparticles. *Ind. Eng. Chem. Res.* **2013**, *52*, 14944–14954. [CrossRef]
12. Sivashankar, R.; Sathya, A.; Vasantharaj, K.; Sivasubramanian, V. Magnetic composite an environmental super adsorbent for dye sequestration—A review. *Environ. Nanotechnol. Monit. Manag.* **2014**, *1–2*, 36–49. [CrossRef]
13. Koivula, R.; Paajanen, A.; Harjula, R.; Lehto, J. Decontamination of radioactive cobalt, nickel, strontium, and cesium from simulate solutions using tin antimonate columns. *Solvent Extr. Ion Exch.* **2003**, *21*, 915–928. [CrossRef]
14. Hung, D.Q.; Dinh, L.X.; Van Tung, N.; Huong, L.T.M.; Lien, N.T.; Minh, P.T.; Le, T.-H. The adsorption kinetic and isotherm studies of metal ions (Co^{2+}, Sr^{2+}, Cs+) on Fe_3O_4 nanoparticle of radioactive importance. *Results Chem.* **2023**, *6*, 101095. [CrossRef]
15. Tayyebi, A.; Outokesh, M.; Moradi, S.; Doram, A. Synthesis and characterization of ultrasound assisted graphene oxide–magnetite" hybrid, and investigation of its adsorption properties for Sr(II) and Co(II) ions. *Appl. Surf. Sci.* **2015**, *353*, 350–362. [CrossRef]
16. Kamel, N.H. Adsorption models of 137Cs radionuclide and Sr (II) on some Egyptian soils. *J. Environ. Radioact.* **2010**, *101*, 297–303. [CrossRef]
17. Chen, C.; Hu, J.; Shao, D.; Li, J.; Wang, X. Adsorption behavior of multiwall carbon nanotube/iron oxide magnetic composites for Ni(II) and Sr(II). *J. Hazard. Mater.* **2008**, *164*, 923–928. [CrossRef]
18. An, Q.; Liu, Q.; Han, C.; Zhao, K.; Sheng, J.; Wei, Q.; Yan, M.; Mai, L. Amorphous vanadium oxide matrixes sup- porting hierarchical porous Fe_3O_4/graphene nanowires as a high-rate lithium storage anode. *Nano Lett.* **2014**, *14*, 6250–6256. [CrossRef]
19. Nene, A.G.; Takahashi, M.; Somani, P.R. Fe_3O_4 and Fe nanoparticles by chemical reduction of fe(acac)3 by ascorbic acid: Role of water. *World J. Nano Sci. Eng.* **2016**, *6*, 20–28. [CrossRef]
20. Jahangiriana, H.; Ismaila, M.H.S.; Haronc, M.D.J.; Moghaddam, R.R.; Shamelie, K.; Hosseinia, S.; Kalantarie, K.; Khandanloue, R.; Gharibshahif, E.; Soltaninejad, S. Synthesis and characterization of zeolite/Fe_3O_4 nanocomposite by green quick precipitation method. *Dig. J. Nanomater. Biostruct.* **2013**, *8*, 1405–1413.
21. Ahmed, S.R.; Cirone, J.; Chen, A. Fluorescent Fe_3O_4 Quantum Dots for H_2O_2 Detection. *ACS Appl. Nano Mater.* **2019**, *2*, 2076–2085. [CrossRef]
22. Gupta, S.; Babu, B. Removal of toxic metal Cr(VI) from aqueous solutions using sawdust as adsorbent: Equilibrium, kinetics and regeneration studies. *Chem. Eng. J.* **2009**, *150*, 352–365. [CrossRef]
23. Lei, T.; Li, S.-J.; Jiang, F.; Ren, Z.-X.; Wang, L.-L.; Yang, X.-J.; Tang, L.-H.; Wang, S.-X. Adsorption of Cadmium Ions from an Aqueous Solution on a Highly Stable Dopamine-Modified Magnetic Nano-Adsorbent. *Nanoscale Res. Lett.* **2019**, *14*, 1–17. [CrossRef]
24. Bagherzadeh, M.; Aslibeiki, B.; Arsalani, N. Preparation of Fe_3O_4/vine shoots derived activated carbon nanocomposite for improved removal of Cr(VI) from aqueous solution. *Sci. Rep.* **2023**, *13*, 3960. [CrossRef] [PubMed]
25. Mirshahghassemi, S.; Lead, J.R. Oil Recovery from Water under Environmentally Relevant Conditions Using Magnetic Nanoparticles. *Environ. Sci. Technol.* **2015**, *49*, 11729–11736. [CrossRef] [PubMed]
26. Hong, J.; Xie, J.; Mirshahghassemi, S.; Lead, J. Metal (Cd, Cr, Ni, Pb) removal from environmentally relevant waters using polyvinylpyrrolidone-coated magnetite nanoparticles. *RSC Adv.* **2020**, *10*, 3266–3276. [CrossRef]
27. Zhang, L.; Wei, J.; Zhao, X.; Li, F.; Jiang, F.; Zhang, M.; Cheng, X. Competitive adsorption of strontium and cobalt onto tin antimonate. *Chem. Eng. J.* **2016**, *285*, 679–689. [CrossRef]
28. Karami, H. Heavy metal removal from water by magnetite nanorods. *Chem. Eng. J.* **2013**, *219*, 209–216. [CrossRef]
29. Fato, F.P.; Li, D.W.; Zhao, L.J.; Qiu, K.; Long, Y.T. Simultaneous Removal of Multiple Heavy Metal Ions from River Water Using Ultrafine Mesoporous Magnetite Nanoparticles. *ACS Omega* **2019**, *4*, 7543–7549. [CrossRef]
30. Zhu, L.; Pan, D.; Ding, L.; Tang, F.; Zhang, Q.; Liu, Q.; Yao, S. Mixed hemimicelles SPE based on CTAB-coated Fe_3O_4/SiO_2 NPs for the determination of herbal bioactive constituents from biological samples. *Talanta* **2010**, *80*, 1873–1880. [CrossRef]
31. Tuutijärvi, T.; Lub, J.; Sillanpää, M.; Chen, G. As(V) adsorption on maghemite nanoparticles. *J. Hazard. Mater.* **2009**, *166*, 1415–1420. [CrossRef] [PubMed]
32. Raju, G.; Holmgren, A.; Forsling, W. Adsorption of Dextrin at Mineral/Water Interface. *J. Colloid Interface Sci.* **1997**, *193*, 215–222. [CrossRef] [PubMed]
33. Anastassakis, G.N. A study on the separation of magnesite fines by magnetic carrier methods. *Colloids Surf. A Physicochem. Eng. Asp.* **1999**, *149*, 585–593. [CrossRef]

34. Belachew, N.; Hinsene, H. Preparation of Zeolite 4A for Adsorptive Removal of Methylene Blue: Optimization, Kinetics, Isotherm, and Mechanism Study. *Silicon* **2022**, *14*, 1629–1641. [CrossRef]
35. Ali, M.M.S.; Sami, N.M.; El Sayed, A.A. Removal of Cs+, Sr^{2+} and Co^{2+} by activated charcoal modified with Prussian blue nanoparticle (PBNP) from aqueous media: Kinetics and equilibrium studies. *J. Radioanal. Nuclear Chem.* **2020**, *324*, 189–201. [CrossRef]
36. Cai, Y.-H.; Yang, X.J.; Schäfer, A.I. Removal of Naturally Occurring Strontium by Nanofiltration/Reverse Osmosis from Groundwater. *Membranes* **2020**, *10*, 321. [CrossRef] [PubMed]
37. van Leeuwen, H.P.; Duval, J.F.L.; Pinheiro, J.P.; Blust, R.; Town, R.M. Chemodynamics and bioavailability of metal ion complexes with nanoparticles in aqueous media. *Environ. Sci. Nano* **2017**, *4*, 2108–2133. [CrossRef]
38. Duval, J.F.L.; Town, R.M.; van Leeuwen, H.P. Lability of nanoparticulate metal complexes at a macroscopic metal responsive (bio)interface: Expression and asymptotic scaling laws. *J. Phys. Chem. C* **2018**, *122*, 6052–6065. [CrossRef]
39. Raji, Z.; Karim, A.; Karam, A.; Khallou, S. Adsorption of Heavy Metals: Mechanisms, Kinetics, and Applications of Various Adsorbents in Wastewater Remediation—A Review. *Waste* **2023**, *1*, 775–805. [CrossRef]
40. Tighadouini, S.; Radi, S.; Roby, O.; Hammoudan, I.; Saddik, R.; Garcia, Y.; Almarhoon, Z.M.; Mabkhot, Y.N. Kinetics, thermodynamics, equilibrium, surface modelling and atomic absorption analysis of selective Cu(II) removal from aqueous solutions and rivers water using silica-2-(pyridin-2-ylmethoxy)ethan-1-ol hybrid material. *RSC Adv.* **2022**, *12*, 611–625. [CrossRef]
41. Sivashankar, R.; Sathya, A.B.; Sivasubramanian, V. Synthesis of magnetic biocomposite for efficient adsorption of azo dye from aqueous solution. *Ecotoxicol. Environ. Saf.* **2015**, *121*, 149–153. [CrossRef] [PubMed]
42. Nithya, R.; Thirunavukkarasu, A.; Sathya, A.B.; Sivashankar, R. Magnetic materials and magnetic separation of dyes from aqueous solutions: A review. *Environ. Chem. Lett.* **2021**, *19*, 1275–1294. [CrossRef]
43. Zhu, W.; Wang, J.; Wu, D.; Li, X.; Luo, Y.; Han, C.; Ma, W.; He, S. Investigating the heavy metal adsorption of mesoporous silica materials prepared by microwave synthesis. *Nanoscale Res. Lett.* **2017**, *12*, 323. [CrossRef] [PubMed]
44. Jahangirian, H.; Rafiee-Moghaddam, R.; Jahangirian, N.; Nikpey, B.; Jahangirian, S.; Bassous, N.; Saleh, B.; Kalantari, K.; Webster, T.J. Green synthesis of zeolite/Fe2O3 nanocomposites: Toxicity & cell proliferation assays and application as a smart iron nanofertilizer. *Int. J. Nanomed.* **2020**, *15*, 1005–1020. [CrossRef]